Generalized Root Raised Cosine Window-based and Prony-Based Estimation Method for OTFS Sensing

Liangchen Sun
Department of Information Science and Technology
Kyushu University, Japan
sun@me.inf.kyushu-u.ac.jp

Yutaka Jitsumatsu
Deptartment of Informatics,
Kyushu University, Japan
jitsumatsu@inf.kyushu-u.ac.jp

***Abstract*—For channel analysis in high-mobility scenarios, accurate estimation of fractional delay–Doppler parameters is essential for reliable sensing and communication. To address this challenge, we explain two novel methods in this paper. First, we introduce a generalized root raised cosine (RRC) window that removes the conventional constraint of keeping window values within $[0, 1]$, allowing negative and greater-than-one values for enhanced waveform flexibility. When combined with the corresponding interpolation algorithm, this method achieves improved sensing capability. In addition, we present a two-stage, Prony-based estimation method that can accurately recover up to $N-1$ delay–Doppler parameters under noiseless conditions. Numerical simulations validate the high estimation accuracy of these approaches and demonstrate their strong potential for future ISAC frameworks.**

***Index Terms*—OTFS, radar, delay Doppler estimation**

I. Introduction

Orthogonal Time-Frequency Space (OTFS) modulation has recently drawn much attention as a robust solution for high-mobility wireless systems due to its strong resilience against Doppler effects and its suitability for doubly dispersive channels [1]–[3]. Beyond traditional signal structure, OTFS has emerged as a promising framework for Integrated Sensing and Communication (ISAC) [4]–[6], offering higher spectral utilization and robustness by merging sensing and communication into a unified structure [7].

A key requirement for both OTFS-based communication and sensing is the accurate estimation of multipath channel parameters, particularly delay and Doppler. When these parameters lie on integer delay-Doppler grid points, estimation is straightforward. However, real propagation conditions typically involve fractional delays and Doppler shifts, which cause energy dispersion across neighboring delay-Doppler bins, generate inter-path interference, and significantly degrade estimation accuracy [8]–[12]. While recent works attempt to mitigate these issues through the method like enhanced correlation methods [13], refined signal modeling [10], analytical investigations [12], or sequential estimation for MIMO-OTFS [14], their performance is often constrained by grid quantization or heavy pilot overhead.

Motivated by these, this work addresses two methods for high-mobility OTFS sensing. First, we consider a waveform that employs a generalized window function derived from the root raised cosine (RRC) [15], which, to the best of our knowledge, have not been systematically utilized for OTFS sensing. Leveraging this waveform, we derive an accurate discrete-time input–output relation that accounts for fractional delay-Doppler parameters. Based on this model, we further show an interpolation technique built upon the autocorrelation of the RRC function, enabling high-precision estimation of fractional delay and Doppler.

Second, we develop a two-stage high-resolution estimation method using Prony's technique [16]. By reorganizing the received OTFS pilot in Time-delay domain, Doppler components are isolated and estimated first by jointly solving several coupled Prony equations. Then delay extraction is also processed by applying the discrete Fourier transform (DFT) and Prony's method. Under noiseless conditions, the Prony method can precisely estimate up to $N-1$ delay-Doppler pairs.

Overall, the generalized window function based waveform design and the Prony-based estimation method each offer distinct advantages for OTFS sensing. Simulation results demonstrate that both approaches can improve the estimation accuracy of fractional delay–Doppler parameters.

The remainder of this paper is organized as follows. Section II presents the waveform design based on the generalized RRC window, derives the corresponding system model, and describes the interpolation method. Section III details the two-stage Prony-based estimation approach, including the separate extraction of Doppler shifts and delays. Section IV provides simulation results and evaluates the performance of two methods. Section V concludes the paper.

II. Channel Estimation Based on a Generalized RRC Window Function

Most OTFS studies use rectangular windows, which are simple but cause spectral leakage and limit sensing resolution. Therefore, in this chapter, we explain a waveform based on generalized RRC window, which has recently been proposed in [15], and demonstrate their advantages for OTFS-based sensing.

A. Flexible Transmission Signal Structure

Let $X_{\mathrm{DD}}[k,\ell]$ denote the symbols in delay–Doppler domain. In this paper, we set $X_{\mathrm{DD}}[k,\ell]$ as a pilot signal

This work was supported in part by JSPS KAKENHI Number JP23K26104 and JP23H00474.

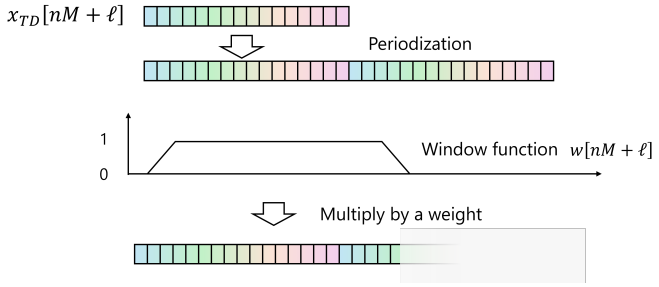

Fig. 1. Illustration of the window function.

expressed as

$$X_{\mathrm{DD}}[k,\ell] = \begin{cases} 1, & k = 0,\ \ell = 0, \\ 0, & \text{otherwise}, \end{cases} \tag{1}$$

to simplify the explanation. Its inverse discrete Zak transform (IDZT) can be expressed as

$$x_{\mathrm{TD}}[nM+\ell] = \frac{1}{\sqrt{N}} \sum_{k=0}^{N-1} X_{\mathrm{DD}}[k,\ell] W_N^{-nk}. \tag{2}$$

In this case, the transmitted signal in time domain can be given by

$$s(t) = \sum_{k=0}^{N-1} \sum_{\ell=0}^{M-1} X_{\mathrm{DD}}[k,\ell]\, h_{k,\ell}(t), \tag{3}$$

where $h_{k,\ell}(t)$ is

$$h_{k,\ell}(t) = \sum_{n=-\infty}^{\infty} w[nM+\ell]\, p\left(t - nT - \frac{\ell T}{M}\right) W_N^{-nk}, \tag{4}$$

with pulse shaping $p(\cdot)$, window function $w[\cdot]$, and DFT twiddle factor $W_N = e^{j2\pi/N}$. Substituting (4) into (3) yields that,

$$\begin{aligned} s(t) &= \sum_{\ell=-\infty}^{\infty} w[\ell]\, x_{\mathrm{TD}}[\ell]\, p(t - \ell T_s) \\ &= \sum_{\ell=-\infty}^{\infty} \tilde{x}_{\mathrm{TD}}[\ell]\, p(t - \ell T_s), \end{aligned} \tag{5}$$

where $\tilde{x}_{\mathrm{TD}}[\ell] = w[\ell] x_{\mathrm{TD}}[\ell]$ and can be better illustrated in Fig. 1. By combining different choices of $w[\cdot]$ and $p(\cdot)$, transmission signals with varying characteristics can be obtained. This structure greatly enhances the flexibility of signal design.

To facilitate the subsequent discussion, several functions are defined first. The rectangular function is defined as

$$\mathrm{rect}(x) = \begin{cases} 1, & |x| < \frac{1}{2}, \\ 0, & |x| > \frac{1}{2}, \\ \frac{1}{2}, & x = \pm\frac{1}{2}. \end{cases} \tag{6}$$

Then the sinc function is given by

$$\mathrm{sinc}(x) = \begin{cases} \dfrac{\sin(\pi x)}{\pi x}, & x \neq 0, \\ 1, & x = 0. \end{cases} \tag{7}$$

Next, the raised cosine (RC) function with roll-off factor β is defined as

$$\mathrm{RC}(f;\beta) = \begin{cases} 1, & |f| < \frac{1-\beta}{2}, \\ \frac{1}{2}\left[1 + \cos\left(\frac{\pi}{\beta}\left(|f| - \frac{1-\beta}{2}\right)\right)\right], & \frac{1-\beta}{2} \le |f| \le \frac{1+\beta}{2}, \\ 0, & |f| > \frac{1+\beta}{2}. \end{cases} \tag{8}$$

The corresponding root raised cosine (RRC) function is expressed as,

$$\mathrm{RRC}(t) = \int_{-\infty}^{\infty} \sqrt{\mathrm{RC}(f)}\, e^{j2\pi t f}\, df. \tag{9}$$

Based on the above functions, the pulse-shaping filters and window functions considered in this work are introduced. Three pulse-shaping filters are considered in the following analysis:

- Rectangular pulse: $p(t) = \mathrm{rect}(t/T_s)$;
- Sinc pulse: $p(t) = \mathrm{sinc}(t/T_s)$;
- RRC pulse with roll-off factor β_p: $p(t) = \mathrm{RRC}(t/T_s;\beta_p)$.

In addition, two types of window functions are employed:

- Rectangular window: $w(t) = \mathrm{rect}(t/(NT))$;
- RRC window with roll-off factor β_w: $w(t) = \mathrm{RRC}(t/((1+\beta_w)NT);\beta_w)$.

The ambiguity functions of $h_{0,0}(t)$ corresponding to different combinations of pulse shapes and window functions are depicted in Fig. 2, where the horizontal and vertical axes represent Doppler and delay, respectively. When a rectangular window is applied, as shown in Fig. 2(a1), (b1), and (c1), noticeable oscillatory behavior appears along the Doppler dimension for all considered pulse shapes. By contrast, employing the RRC window in conjunction with a rectangular pulse, as illustrated in Fig. 2(a2), effectively suppresses these oscillations. This property is particularly beneficial, as it leads to a more regular ambiguity structure and simplifies subsequent processing in the delay-Doppler domain. Therefore, the RRC window combined with rectangular pulse is employed throughout the following analysis.

B. Corresponding Receive Signal and Channel Estimation

Assume the number of reflected echoes received by antenna is P. For the i-th echo, let α_p, $t_{D,p}$, and $f_{D,p}$ denote its attenuation, delay, and Doppler shift. The noise-free received signal is

$$r(t) = \sum_{p=0}^{P-1} \alpha_p\, s(t - t_{D,p})\, e^{j2\pi f_{D,p} t}. \tag{10}$$

Here, the delay and Doppler frequency are defined as $t_{d,p} = (l + \varepsilon_t)T_s$ and $f_{D,p} = \frac{k+\varepsilon_f}{NMT_s}$, where l and k are the integer parts, ε_t and ε_f are the fractional parts.

In addition, we assume that the delay lengths satisfy $T_B < t_{d,p} < (U-1)T_B$ to avoid additional interference. T_B is the interval of an OTFS block, UT_B is the pulse repetition interval (PRI), and the next OTFS block is transmitted after a silent

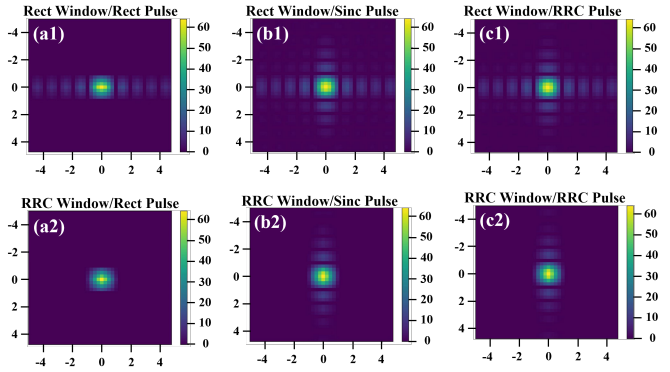

Fig. 2. The fine ambiguity function $A_{s,s}(\tau,\nu)$ is illustrated for $-5T_s < \tau < 5T_s$ and $-5/T_B < \nu < 5/T_B$ under different pulse shaping schemes, including (a) rectangular, (b) sinc, and (c) RRC pulses. The RRC pulse employs a roll-off factor of 25%. In addition, $(x1)$ and $(x2)$ indicate rectangular and RRC windowing, respectively [15].

period lasting $(U-1)T_B$. The Doppler range is restricted by the sampling period T_s, i.e., $2f_{D,\max} < 1/T_s$.

The received $r(t)$ signal is passed through the matched filter $\hat{p}(t) = \overline{p(-t)}$ and sampled at $t = \ell T_s$, yielding

$$y_{\mathrm{TD}}[\ell] = \int_{-\infty}^{\infty} r(t)\,\hat{p}(t-\ell T_s)\,\mathrm{d}t, \tag{11}$$

where ℓ ranges from $\lfloor(1+\beta_w)NM\rfloor$ to $\lfloor(U-(1+\beta_w))NM\rfloor$, and β_w is the excess bandwidth ratio.

The discrete-time discrete-frequency cross-ambiguity function is then calculated as,

$$A_{y,x}[k,\ell] = \frac{1}{\sqrt{NM}} \sum_{\ell'} y_{\mathrm{TD}}[\ell'+\ell]\tilde{x}_{\mathrm{TD}}[\ell']W_{NM}^{k\ell'}, \tag{12}$$

where ℓ' denotes the index of DFT of $y_{\mathrm{TD}}[\ell'+\ell]\tilde{x}_{\mathrm{TD}}[\ell']$. By locating the peak $A_{y,x}[\hat{k},\hat{\ell}]$, the integer parts of the delay–Doppler parameters can be estimated. However, due to the fractional delay–Doppler components, the true peak does not lie exactly on $A_{y,x}[\hat{k},\hat{\ell}]$ but rather in its vicinity. By comparing the magnitudes of the neighboring grid points, the four grid points surrounding the actual peak can be identified, forming the following local matrix,

$$\begin{bmatrix} |A_{y,x}[\hat{k},\hat{\ell}]| & |A_{y,x}[\hat{k},\hat{\ell}+1]| \\ |A_{y,x}[\hat{k}+1,\hat{\ell}]| & |A_{y,x}[\hat{k}+1,\hat{\ell}+1]| \end{bmatrix}, \tag{13}$$

which is denoted as $\begin{bmatrix} A_{00} & A_{01} \\ A_{10} & A_{11} \end{bmatrix}$.

Next, the interpolation method is used for fractional parameter estimation. By substituting (5) into (10) and then substituting the result into (11), we can obtain that,

$$y_{\mathrm{TD}}[\ell] = \sum_{p=0}^{P-1} \alpha_p \sum_{\ell'} \tilde{x}_{\mathrm{TD}}[\ell'] e^{j\pi f_{D,p}(\ell+\ell')T_s} \cdot A_{pu,pu}((\ell-\ell')T_s - t_{D,p}, -f_{D,p}). \tag{14}$$

where $A_{pu,pu}((\ell-\ell')T_s - t_{D,p}, -f_{D,p})$ is the autocorrelation function of the pulse and can be further approximated as $\approx pu * \hat{pu}((\ell-\ell')T_s - t_{D,p})$ since $|f_{D,p}|$ has been considered much smaller than $1/T_s$. In this case, it can be observed that (12) can be approximately regarded as the autocorrelation function of (5) with an attenuation coefficient, denoted by $\alpha \cdot A_{ss}$. The detailed derivation is omitted here due to space limitations. Therefore, a total error function is defined as

$$L(\alpha,\varepsilon_t,\varepsilon_f) = \sum_{i=0}^{1}\sum_{j=0}^{1} \left|A_{ij} - \alpha \cdot A_{ss}(i-\varepsilon_t, j-\varepsilon_f)\right|^2. \tag{15}$$

Since X_{DD} is the pilot signal shown in (1), the A_{ss} can be further approximated by

$$A_{ss}(\tau,\nu) \approx pu * \hat{pu}(\tau) \cdot W * \hat{W}(\nu), \quad |\tau| \le T_s,\ |\nu| \le \frac{1}{NT}. \tag{16}$$

For the adopted RRC window, the autocorrelation function can be expressed as,

$$W*\hat{W}(\nu) = \begin{cases} \frac{1}{2}\cos(b\nu)(1-2\nu-2a) + \frac{1}{2b}\sin(b-b\nu-2ba) \\ \quad -\frac{3}{2b}\sin(-b\nu) + 2a - \nu, \quad \text{for: } 0 \le \nu \le -a+\frac{1}{2} \\ \frac{2}{b}\sin\left(\frac{b}{2}-ba\right) + 2a - \nu, \quad \text{for: } -a+\frac{1}{2} < \nu \le 2a \\ \frac{2}{b}\left[\sin\left(\frac{b}{2}-ba\right) - \sin(-2ba+b\nu)\right] \\ + \frac{1}{4b}\left[\sin(-2ba+b\nu) - \sin(2b(a-\nu)+b\nu)\right] \\ + \frac{1}{2}\cos(b\nu-2ba)(-2a+\nu), \quad \text{for: } 2a < \nu \le a+\frac{1}{2} \\ \frac{1}{2}\left[\frac{1}{b}\sin(b-b\nu) + \cos(-2ba+b\nu)(-\nu+1)\right], \\ \quad \text{for: } a+\frac{1}{2} < \nu \le 1 \\ 0, \quad \text{for: otherwise,} \end{cases} \tag{17}$$

where $a = \frac{1-\beta}{2(1+\beta)}$, $b = \frac{\pi(1+\beta)}{2\beta}$, and β is chosen to be 0.25 in this work. By substituting (13) into (15), the desired fractional parameters $(\hat{\varepsilon}_t, \hat{\varepsilon}_f)$ as well as the attenuation factor $\hat{\alpha}$ can be obtained via $\arg\min_{\alpha,\varepsilon_t,\varepsilon_f} L(\alpha,\varepsilon_t,\varepsilon_f)$. The whole process is summarized in Algorithm 1.

Algorithm 1 Channel Estimation Based on a Generalized RRC Window Function

Require: Transmitted signal samples $x_{\mathrm{TD}}[\ell]$ over the transmission interval and received samples y_{TD} over the observation window. Specify the parameter MAX_PATHS.

1: Evaluate the ambiguity function in (12) by applying an NM-point FFT to each product sequence $y_{\mathrm{TD}}[\cdot+\ell]\,x_{\mathrm{TD}}[\cdot]$.
2: Identify the MAX_PATHS index pairs $[\hat{k},\hat{\ell}]$ associated with the largest magnitudes of $A_{y,x}[k,\ell]$, and collect them into a candidate set denoted by $\{[\hat{k},\hat{\ell}]\}$.
3: Perform peak extraction on $|A_{y,x}[\hat{k},\hat{\ell}]|$ by detecting local maxima above a threshold and determining their associated 2×2 submatrices $\{A_{00}, A_{01}, A_{10}, A_{11}\}$.
4: Based on (16) and use `optimize.minimize` to solve a least-squares problem between the interpolated values and the obtained 2×2 matrix.
5: **return** $(\hat{\varepsilon}_t, \hat{\varepsilon}_f)$ and $\hat{\alpha}$.

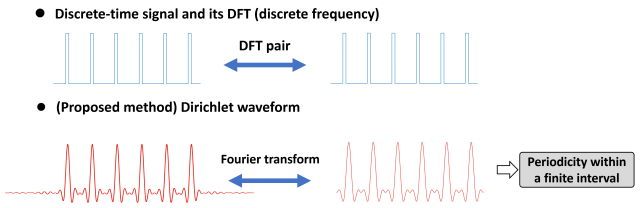

Fig. 3. Time- and frequency-domain illustrations of the Dirichlet waveform used as the transmit signal [16].

III. Channel Estimation Based on Prony method

In this chapter, we explain a two-stage Prony-based method which has recently been proposed in [16]. The method improves robustness in multipath channels while reducing computational cost. A DFT-friendly pilot is designed to preserve signal periodicity, and the received samples are arranged into a time-delay domain matrix. This enables the core advantage of our approach: Doppler and delay are estimated separately—Doppler first, then delay after compensation.

A. Signal Structure

A center-shifted variant of the Dirichlet kernel is chosen as the transmitted pilot waveform,

$$s(t) = D_M\left(\frac{t}{T}\right) w(t), \tag{18}$$

$$D_M(x) = \sum_{m=-M/2}^{M/2-1} e^{j2\pi mx} = e^{-j\pi x}\frac{\sin(\pi Mx)}{\sin(\pi x)}, \tag{19}$$

for it enables efficient DFT-based reception. In contrast to the method in Section II, the window function $w(t)$ used here is a rectangular window of duration NT, where T is the time-slot duration and N is the number of pilot repetitions. The function $D_M(t/T)$ exhibits discrete spectral components at frequencies $f = m/T$, $m = -M/2, \ldots, M/2-1$. Figure 3 illustrates the signal structure. In addition, we also use the X_{DD} defined in (1) to simplify the analysis.

For the received continuous-time signal, its expression is same as (10). When sampling at interval $T_s = T/M$, it can be given by

$$r_{\mathrm{TD}}[\ell] = \int r(t)\,\mathrm{sinc}\left(\frac{t}{T_s} - \ell\right) \mathrm{d}t \approx r(\ell T_s), \tag{20}$$

where $\mathrm{sinc}(x) = \frac{\sin(\pi x)}{\pi x}$. This approximation holds when the maximum Doppler shift satisfied $f_{D,\max} < 1/T$ is sufficiently small compared to the transmit signal bandwidth $1/T_s = M/T$.

B. Problem Formulation

A general challenge is that fractional delay and Doppler must be jointly estimated, as they are strongly coupled in the received signal. Under such coupling, separate estimation suffers from interference and reduced accuracy, while joint estimation—though capable of addressing these issues—requires extremely fine resolution in the analysis process. This results in high computational complexity and long processing time, limiting its applicability in time-critical scenarios such as V2V communications. Thus, we give the following lemma.

Lemma 1: Consider the $N \times M$ matrix $\boldsymbol{R} = (R_{n,\ell})$ whose entries are given by

$$R_{n,\ell} = r_{\mathrm{TD}}[\,nM + \ell\,].$$

Define $\boldsymbol{E} \in \mathbb{C}^{N\times P}$ by

$$E_{n,p} = e^{j2\pi f_{D,p} nT},$$

and let $\boldsymbol{V} = (V_{p,\ell}) \in \mathbb{C}^{P\times M}$ with

$$V_{p,\ell} = \alpha_p\, D_M\left(\frac{\ell}{M} - \frac{t_{d,p}}{T}\right) e^{j2\pi f_{D,p}\ell T_s}.$$

Then the matrix $\boldsymbol{R}$ admits the factorization

$$\boldsymbol{R} = \boldsymbol{E}\,\boldsymbol{V}. \tag{21}$$

The proof is omitted for brevity. From the above lemma, it can be seen that the matrix $\mathbf{E}$ is determined solely by the Doppler shifts $f_{D,p}$, regardless of the delays $t_{d,p}$. Once the Doppler shifts $f_{D,p}$ are accurately estimated, the Doppler components contained in $\mathbf{V}_{p,\ell}$ can be compensated. Consequently, we obtain a Doppler-free matrix $\widetilde{\mathbf{V}}_{p,\ell}$, expressed as

$$\widetilde{V}_{p,\ell} = \alpha_p D_M\left(\frac{\ell}{M} - \frac{t_{d,p}}{T}\right), \tag{22}$$

where $\ell = 0, 1, \ldots, M-1$.

Furthermore, applying an M-point DFT to $\widetilde{V}_{p,\ell}$, $\ell = 0, 1, \ldots, M-1$ yields

$$\begin{aligned}
&\sum_{\ell=0}^{M-1} \widetilde{V}_{p,\ell}\, e^{-j\frac{2\pi}{M}m\ell} \\
&= \sum_{\ell=0}^{M-1} \alpha_p D_M\left(\frac{\ell}{M} - \frac{t_{d,p}}{T}\right) e^{-j\frac{2\pi}{M}m\ell} \\
&= \alpha_p \sum_{m'=-\frac{M}{2}}^{\frac{M}{2}-1} \sum_{\ell=0}^{M-1} e^{j2\pi m'\left(\frac{\ell}{M} - \frac{t_{d,p}}{T}\right)} e^{-j\frac{2\pi}{M}m\ell} \\
&= \alpha_p M e^{-j2\pi m'\frac{t_{d,p}}{T}},
\end{aligned} \tag{23}$$

where $m' = m$ for $0 \le m \le \frac{M}{2} - 1$, and $m' = m - M$ for $\frac{M}{2} \le m \le M-1$.

Through this procedure, the originally coupled Doppler–delay parameters are effectively decoupled, and the resulting expression exhibits a similar exponential structure. The advantage of this decoupling is that it transforms the joint estimation problem into a set of one-dimensional spectral estimation problems, enabling the use of many classical high-resolution techniques such as ESPRIT, MUSIC, and Prony.

In this work, we adopt Prony's method due to its ability to provide super-resolution parameter estimation with low computational complexity, while avoiding the eigen-decomposition required in subspace-based approaches. Moreover, Prony's method directly exploits the exponential structure of $E_{n,p}$ and $\widetilde{V}_{p,\ell}$, making it particularly well suited for the above estimation procedure.

C. Prony Based Channel Estimation

This section presents the Prony-based method [16]. Corresponding to the Section III-B, the overall procedure consists of three estimation stages: Doppler estimation, preprocessing for delay estimation, and delay estimation.

1) Stage 1 - Doppler Estimation: Doppler shifts are first estimated in this stage. Since $\boldsymbol{R} \in \mathbb{C}^{N\times M}$ contains M columns, we apply Prony's method to each column independently. The resulting Prony polynomials share the same roots, which correspond to the Doppler frequencies. Thus, the M columns provide M coupled equations, leading to a more robust Doppler estimation.

We set the predicted number of paths to $\hat{P}$ with $\hat{P} < N-1$. A key challenge in this method lies in accurately estimating the predicted number of paths, $\hat{P}$. This parameter directly determines the structure of the polynomial in (29), and therefore has a critical impact on the accuracy of the subsequent Doppler estimation. Choosing an appropriate information criterion is a common challenge in hyperparameter estimation. Although information-theoretic criteria such as the Akaike Information Criterion (AIC) [17] and the Bayesian Information Criterion (BIC) [18] are frequently used, they may fail to provide reliable estimates in certain scenarios. To address this limitation, we adopt a simple energy-based thresholding rule to determine $\hat{P}$, which yields more stable and accurate results. Due to space constraints, the detailed analysis and comparison are omitted here and can be found in [16].

Based on $\hat{P}$, Toeplitz matrix $T^{(\ell)}$ for each $\ell = 0, 1, \ldots, M-1$ is constructed as,

$$T^{(\ell)} = \begin{pmatrix} R_{\hat{P},\ell} & R_{\hat{P}-1,\ell} & \cdots & R_{0,\ell} \\ R_{\hat{P}+1,\ell} & R_{\hat{P},\ell} & \cdots & R_{1,\ell} \\ \vdots & \vdots & & \vdots \\ R_{N-1,\ell} & R_{N-2,\ell} & \cdots & R_{N-\hat{P}-1,\ell} \end{pmatrix}, \tag{24}$$

and stacked vertically to form the merged matrix,

$$T = \begin{bmatrix} T^{(0)} \\ \vdots \\ T^{(M-1)} \end{bmatrix}. \tag{25}$$

Next, we determine a vector $\boldsymbol{a} = (a[0], a[1], \ldots, a[\hat{P}])^t$ with $a[0] = 1$ that satisfies

$$\mathbf{T}\,\boldsymbol{a} = \mathbf{0}, \qquad \mathbf{0} \in \mathbb{C}^{M(N-\hat{P})}. \tag{26}$$

Let $\boldsymbol{t}_0$ be the first column of $\mathbf{T}$, and let $\widetilde{\mathbf{T}}$ be the matrix obtained by removing this column. The vector $\boldsymbol{a}$ can be obtained by

$$\boldsymbol{a}^t = (1,\, \tilde{\boldsymbol{a}}^t), \tag{27}$$

$$\tilde{\boldsymbol{a}} = -\widetilde{\mathbf{T}}^{\dagger}\boldsymbol{t}_0, \tag{28}$$

where $\widetilde{\mathbf{T}}^{\dagger}$ denotes a generalized inverse.

Then, the roots of the Prony polynomial composed by $\boldsymbol{a}$,

$$a[0]x^{\hat{P}} + a[1]x^{\hat{P}-1} + \cdots + a[\hat{P}-1]x + a[\hat{P}] = 0. \tag{29}$$

are found, denoted as Z_p for $p = 1, 2, \ldots, \hat{P}$. In this case, the estimated Doppler frequencies are given by

$$\hat{f}_{D,p} = \frac{\arg(Z_p)}{2\pi T}, \tag{30}$$

where $\arg(\cdot)$ denotes the complex argument.

2) Stage 2 - Preprocessing for Delay Estimation: The matrix $\hat{\boldsymbol{E}}$ is first reconstructed based on the $\hat{f}_{D,p}$, expressed as

$$\hat{\boldsymbol{E}} = \left(e^{j2\pi \hat{f}_{D,p} nT}\right)_{n,p}. \tag{31}$$

Next, $\boldsymbol{V}$ is estimated according to (21), shown as

$$\hat{\boldsymbol{V}} = \arg\min_{\boldsymbol{V}} \left\| \boldsymbol{R} - \hat{\boldsymbol{E}}\boldsymbol{V} \right\|^2 = \hat{\boldsymbol{E}}^{\dagger}\boldsymbol{R}, \tag{32}$$

where $\dagger$ denotes the Moore–Penrose pseudo-inverse.

By applying the estimated Doppler shifts $\hat{f}_{D,p}$ once more, the Doppler components in $\hat{\mathbf{V}}$ are removed, resulting in a matrix $\widetilde{\mathbf{V}}$ with only the delay components shown as,

$$\widetilde{V}_{p,\ell} = \hat{V}_{p,\ell}\, e^{-j2\pi \hat{f}_{D,p}\ell T_s}. \tag{33}$$

Assuming that the $\hat{f}_{D,p}$ are accurate, (33) reduces to (22). In that case and based on (23), by applying the M-point DFT to each row of $\widetilde{\mathbf{V}}$, we obtain

$$Y_p[m] = \alpha_p M\, e^{-j2\pi m t_{d,p}/T}, \tag{34}$$

for $m = -\frac{M}{2}, \ldots, \frac{M}{2}-1$. Then the time delay can be estimated.

3) Stage 3: Delay Estimation: Let L denote the number of paths sharing the same Doppler shift and simply set $L = 1$ in all simulations. This assumption may be restrictive when Doppler shifts are nearly identical, but remains acceptable at high SNR.

Similarly to stage 1, for each $\boldsymbol{Y}_p = (Y_p[m])_m$, the Toeplitz matrix is first constructed as,

$$(\boldsymbol{T}')_{ij} = Y_p\left[L - \frac{M}{2} + i - j\right], \tag{35}$$

where $i = 1, \ldots, M-1$ and $j = 1, 2$.

Then, a nonzero vector $\boldsymbol{a'} = (a'[0], a'[1])^t$ satisfying $\boldsymbol{T'a'} = \mathbf{0}$ is obtained, and the roots of the polynomial, $a'[0]x + a'[1] = 0$, formed by $\boldsymbol{a'}$ are computed and denoted as $Z_{p,\ell}$.

Under this condition, the estimated delays are

$$\hat{t}_{d,p,\ell} = \frac{\arg(Z_{p,\ell})}{2\pi} T. \tag{36}$$

IV. Numerical Results

Numerical simulations are conducted with $T = 10^{-6}$ seconds and $N = M = 32$. The delays and Doppler shifts are uniformly generated over $[0, T]$ and $[-1/(2T),\, 1/(2T)]$, and the corresponding estimation results are illustrated in Fig. 4. Here, we evaluated the performance of the two methods in terms of the matching map and the root-mean-square error (RMSE). The results presented in the matching maps are normalized by the corresponding resolutions $\Delta_t = T/M$ and $\Delta_f = 1/NT$; that is, both the true parameters and the estimates are divided

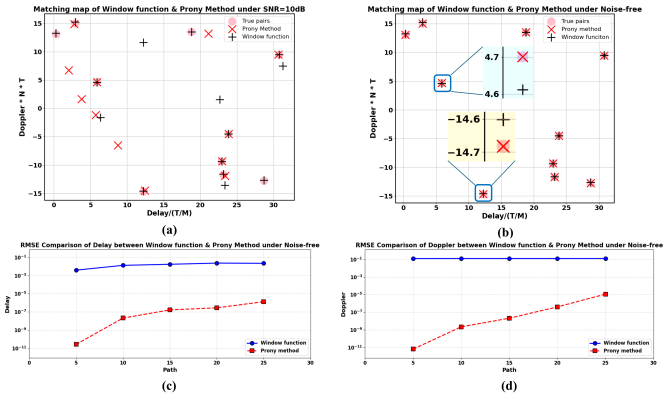

Fig. 4. Estimation performance of the window-function (WF) method and the Prony method. (a) Matching maps at SNR = 10 dB; (b) Matching maps in the noise-free case; (c) RMSE of delay estimation in the noise-free case over 200 Monte Carlo trials; (d) RMSE of Doppler estimation in the noise-free case over 200 Monte Carlo trials.

by their respective resolutions. In addition, the RMSE is computed as RMSE $= \sqrt{\frac{1}{run \cdot P} \sum_{n=1}^{run} \sum_{p=1}^{P} \left(\hat{x}_{n,p} - x_{n,p}\right)^2}$, where run, x_p and $\widehat{x}_p$ denote the number of Monte Carlo trials, true and estimated parameters.

Figure 4 shows that, in the noise-free case, the Prony method provides highly accurate estimates for both delay and Doppler. The window-function (WF) method, while more robust in low-SNR situations, exhibits a small inherent estimation bias, which is also reflected in the RMSE results obtained over 200 Monte Carlo trials.

In terms of computational cost, the Prony method requires 0.0809 seconds, whereas the WF method requires 1.2969 seconds on the same device (measured via `time.time`). This highlights a trade-off between computational efficiency and robustness across the two approaches.

Looking ahead, two directions are of particular interest: (i) improving the noise robustness of the Prony method, and (ii) developing more efficient and accurate algorithms for estimating the number of propagation paths.

V. Conclusion

This paper has introduced two high-mobility OTFS sensing methods [15], [16]. The generalized RRC window, together with an autocorrelation-based interpolation technique, enhances fractional delay–Doppler estimation through improved waveform shaping. In contrast, the two-stage Prony-based method enables high-resolution parameter recovery. Simulation results demonstrate that the generalized RRC window-based method is more robust at low SNR, whereas the Prony-based method achieves higher estimation accuracy with lower computational complexity, highlighting their potential for future OTFS-based ISAC systems.

References

[1] R. Hadani, S. Rakib, M. Tsatsanis, A. Monk, A. J. Goldsmith, A. F. Molisch, and R. Calderbank, "Orthogonal time frequency space modulation," in *2017 IEEE Wireless Communications and Networking Conference (WCNC)*. IEEE, 2017, pp. 1–6.

[2] S. K. Mohammed, R. Hadani, A. Chockalingam, and R. Calderbank, "OTFS—a mathematical foundation for communication and radar sensing in the delay-Doppler domain," *IEEE BITS the Information Theory Magazine*, vol. 2, no. 2, pp. 36–55, 2022.

[3] ——, "OTFS—predictability in the delay-doppler domain and its value to communication and radar sensing," *IEEE BITS the Information Theory Magazine*, vol. 3, no. 1, pp. 56–75, 2023.

[4] W. Yuan, Z. Wei, S. Li, J. Yuan, and D. W. K. Ng, "Integrated sensing and communication-assisted orthogonal time frequency space transmission for vehicular networks," *IEEE Journal of Selected Topics in Signal Processing*, vol. 15, no. 6, pp. 1515–1528, 2021.

[5] Y. Shi and Y. Huang, "Integrated sensing and communication-assisted user state refinement for OTFS systems," *IEEE Trans. Wireless Comm.*, vol. 23, no. 2, pp. 922–936, 2023.

[6] H. I. Hegazy, A. Mohamed, I. Al-Nahhal, and O. A. Dobre, "Low complexity super-resolution otfs-assisted isac framework for thz communication," *IEEE Transactions on Vehicular Technology*, 2025.

[7] M. Ahmadipour, M. Kobayashi, M. Wigger, and G. Caire, "An information-theoretic approach to joint sensing and communication," *IEEE Trans. Inform. Theory*, vol. 70, no. 2, pp. 1124–1146, 2022.

[8] L. Gaudio, M. Kobayashi, G. Caire, and G. Colavolpe, "On the effectiveness of OTFS for joint radar parameter estimation and communication," *IEEE Trans. Wireless Comm.*, vol. 19, no. 9, pp. 5951–5965, 2020.

[9] S. K. Dehkordi, L. Gaudio, M. Kobayashi, G. Colavolpe, and G. Caire, "Beam-space mimo radar with OTFS modulation for integrated sensing and communications," in *2022 IEEE Int. Conf. on Comm. Workshops (ICC Workshops)*. IEEE, 2022, pp. 509–514.

[10] K. Zhang, W. Yuan, S. Li, F. Liu, F. Gao, P. Fan, and Y. Cai, "Radar sensing via OTFS signaling: A delay doppler signal processing perspective," in *ICC 2023-IEEE Int. Conf. Comm.*, 2023, pp. 6429–6434.

[11] Y. Wu, C. Han, and Z. Chen, "DFT-spread orthogonal time frequency space system with superimposed pilots for terahertz integrated sensing and communication," *IEEE Trans. Wireless Comm.*, vol. 22, no. 11, pp. 7361–7376, 2023.

[12] O. Zacharia and M. V. Devi, "Fractional delay and doppler estimation for OTFS based ISAC systems," in *2023 IEEE Wireless Communications and Networking Conference (WCNC)*, 2023, pp. 1–6.

[13] S. P. Muppaneni, S. R. Mattu, and A. Chockalingam, "Channel and radar parameter estimation with fractional delay-doppler using OTFS," *IEEE Communications Letters*, vol. 27, no. 5, pp. 1392–1396, 2023.

[14] K. R. R. Ranasinghe, H. S. Rou, and G. T. F. de Abreu, "Fast and efficient sequential radar parameter estimation in mimo-otfs systems," in *ICASSP 2024-2024 IEEE Int. Conference on Acoustics, Speech and Signal Processing (ICASSP)*. IEEE, 2024, pp. 8661–8665.

[15] L. Sun and Y. Jitsumatsu, "Design of otfs signals with pulse shaping and window function for otfs-based radar systems," in *2025 IEEE VTS Asia Pacific Wireless Communications Symposium (APWCS)*. IEEE, 2025, pp. 1–5.

[16] Y. Jitsumatsu and L. Sun, "Two-stage prony-based estimation of fractional delay and doppler shifts in otfs modulation," *arXiv preprint arXiv:2506.17599*, 2025.

[17] H. Akaike, "A new look at the statistical model identification," *IEEE transactions on automatic control*, vol. 19, no. 6, pp. 716–723, 2003.

[18] G. Schwarz, "Estimating the dimension of a model," *The annals of statistics*, pp. 461–464, 1978.